



**HAL**  
open science

# Thermally-induced cracks and their effects on natural and industrial geomaterials

Naïma Belayachi, Céline Mallet, Mounir El Marzak

## ► To cite this version:

Naïma Belayachi, Céline Mallet, Mounir El Marzak. Thermally-induced cracks and their effects on natural and industrial geomaterials. *Journal of Building Engineering*, 2019, 25, pp.100806. 10.1016/j.jobe.2019.100806 . hal-02170469

**HAL Id: hal-02170469**

**<https://univ-orleans.hal.science/hal-02170469>**

Submitted on 25 Oct 2021

**HAL** is a multi-disciplinary open access archive for the deposit and dissemination of scientific research documents, whether they are published or not. The documents may come from teaching and research institutions in France or abroad, or from public or private research centers.

L'archive ouverte pluridisciplinaire **HAL**, est destinée au dépôt et à la diffusion de documents scientifiques de niveau recherche, publiés ou non, émanant des établissements d'enseignement et de recherche français ou étrangers, des laboratoires publics ou privés.



Distributed under a Creative Commons Attribution - NonCommercial 4.0 International License

1 Journal of Building Engineering

2

## 3 Thermally-induced cracks and their effects on natural and 4 industrial geomaterials

5

6 Naima Belayachi<sup>(1)</sup>, Céline Mallet<sup>(1)</sup>, Mounir El Marzak<sup>(2)</sup>

7

8

### 9 Abstract

10 Thermal stress can result in significant changes in the mechanical and transport properties of  
11 building materials, especially in terms of cracking. Three building materials were studied: two  
12 concretes, a siliceous and a calcareous one, and a natural calcareous rock, the Tuffeau. The samples  
13 were subjected to thermal shock, repetitive heating-cooling cycles, and high temperature heating in  
14 order to analyze the effects of maximum temperature, cooling rate, and repetitive heating on the  
15 three materials. The induced cracks were then characterized by physical and hydraulic  
16 measurements, namely elastic wave velocities, porosity and effective thermal conductivity. Elastic  
17 wave velocities were used to determine crack density while effective thermal conductivity was used  
18 to determine crack connectivity. Cracks were also quantitatively described through direct  
19 microstructural observations using scanning electron microscopy. Results show the effectiveness of  
20 the different protocols in inducing cracks. Unexpectedly, repetitive heating-cooling cycles caused  
21 the most significant sample damage, whatever the sample. A second main result is based on the  
22 comparison of the different materials. It was found that the behavior of the two concretes was very  
23 similar: the stronger the thermal treatment, the more the crack density and connectivity increased,  
24 albeit with a slight difference in that the siliceous concrete appeared to be less resistant to sharp  
25 thermal variations. This is interpreted as being linked to microstructural effects: in the siliceous  
26 concrete, we observed cracks that nucleated around and inside grains, but not in the calcareous  
27 concrete. Lastly, the behavior of the Tuffeau limestone was different from that of the concretes:  
28 when crack density increased, the crack connectivity and the porosity both decreased. This different  
29 behavior is interpreted in the light of microstructural observations of the crack apertures: the  
30 thermally induced cracks in Tuffeau are too small to influence the effective thermal connectivity  
31 measurement and to allow fluid flow during the porosity measurement, whereas in the concretes,  
32 cracks were observed to be much more open. As an outlook, we discuss a possible equivalent test to  
33 the normalized fire protocol, performed at high temperature, to test the fire resistance of materials.

34

35 Key words: Thermal treatment; Thermal cracking; Calcareous concrete; Siliceous concrete; Tuffeau  
36 limestone; geophysical characterization

37

---

38 Corresponding author: Céline Mallet

39 E-mail: [celine.mallet@univ-orleans.fr](mailto:celine.mallet@univ-orleans.fr)

40 Tel.: +33 023 849 45 96

41

42 <sup>(1)</sup> Université d'Orléans, Université de Tours, INSA Centre Val de Loire - Laboratoire de Mécanique  
43 Gabriel Lamé

44 Polytech Orléans, 8 rue Léonard de Vinci, 45072 Orléans, France

45 <sup>(2)</sup> Faculté des Sciences et Techniques de Tanger (FSTT), Maroc

46

## 1. Introduction

Cracks reduce the resistance and rigidity of materials, contribute to the deterioration of civil engineering structures, change the material properties and compromise the safety and stability of structures. Cracking can be caused by fatigue to repetitive loading (Kong and Li, 2019), or by accidental or natural thermal variations (Belayachi *et al.*, 2012; Samouh *et al.*, 2019; Li *et al.*, 2019). In the case of the accidental huge thermal variation due to fire, it has been observed that a great amount of damage may also come from rapid cooling (Botte and Caspeepe, 2017). All these conditions have a strong impact on the functionality of the structural elements as they significantly reduce the material's performance. Thermally induced cracks can, for example, increase the permeability of materials, which may increase the transport of aggressive agents (Hoseini *et al.*, 2009; Wang *et al.*, 2019). The most severe thermal condition for building materials is exposure to fire (Sarker *et al.*, 2014), and several studies have been performed to assess the fire resistance of structural elements (Shah and Sharma, 2017; Li *et al.*, 2018). However, it is essential to understand the causes of the thermally induced cracks of materials frequently used in buildings under various thermal conditions and not only in the extreme case of fire. Studying the effect of cracking is very beneficial for project design as thermal effects raise many engineering issues that need to be addressed in order to ensure resistance to fire or to seasonal variations in temperature (Xiong and Liew, 2016 ; Novák and Kohoutková, 2017).

In the laboratory, the crack networks introduced by thermal stress are studied using different protocols to represent the impact of fire, the rapid cooling and the seasonal temperature variations (Lam Dos Santos *et al.*, 2011). Rapid cooling is studied thanks to a protocol of thermal shocks (Yavuz *et al.*, 2006), while seasonal variations are studied through progressive heating-cooling cycles (Khan *et al.*, 2010; Lam Dos Santos *et al.*, 2011). Some high temperature tests (Liu and Xu, 2015; Khan and Abbas, 2016; Liu *et al.*, 2018), and normalized thermal treatments (ISO1999) can be found in the literature to study the behavior of materials under extreme conditions. The objective of these protocols is to determine the material strength under fire conditions (Xiong and Liew, 2016; Novák and Kohoutková, 2017). However, these useful protocols are constraining due to the material required (an accurate high temperature oven). In addition, an accurate temperature curve has to be followed (ISO1999 and Yermak *et al.*, 2017). For these reasons, despite the importance of the topic, few studies are reported in the literature on concrete or other building materials, especially at high temperature (Mindeguia *et al.*, 2010; Kodur and Agrawal, 2017). There is therefore a need for an equivalent protocol to high temperature procedures in order to correlate the results with tests simulating fire conditions.

The occurrence of thermally induced cracks is dependent upon the temperature, thermal expansion, initial porosity and grain size of the material (Liu *et al.*, 2018). In addition, the damage due to cracks under temperature variation is a complex mechanism that involves a mixture of chemical, physical and mechanical processes (Ghazi Wakili *et al.*, 2007). Thus, it is important to study the mechanisms of thermally-induced cracks in different materials.

Concrete is the most widely studied material because of its extensive use in different structures and its low reaction to high thermal stress. Moreover, because of its low heating rate, concrete does not reach temperatures that affect its mechanical characteristics. However, surface cracking and spalling can lead to weakening of its properties (Yermak *et al.*, 2017).

In traditional buildings, limestone is also often used, especially for its local availability. This calcareous rock can be affected by temperature variations (sharp or not), which can lead to building instabilities. Indeed, Al-Omari *et al.* (2014) showed that when coupled to a salt pollutant, heating-cooling cycles can be highly destructive for these calcareous stones. In addition, cracks are observed on the wall surfaces and stone spalling is often present (Beck *et al.*, 2016). It is therefore crucial to study stone decay due to thermal variation in heritage buildings.

1  
2  
3 It is important to be able to characterize cracks using non-destructive physical measurements in  
4 order to be able to reproduce these measurements in the field. In the present study, elastic wave  
5 velocity measurements were used to characterize the thermally induced crack networks. These  
6 geophysical measurements allow for describing the crack density, a physical damage parameter  
7 introduced by Walsh (1965a, b) (see the recent review by Guéguen and Kachanov, 2011). In  
8 addition, more recently, measurements of electric or thermal conductivities are often considered in  
9 order to describe the material transport properties (Han *et al.*, 2015), especially the crack network  
10 connectivity. Porosity and microstructural observations were also carried out in order to complete  
11 the crack characterization.

12  
13 The study has two main objectives: (i) to compare the crack network characteristics introduced by  
14 different thermal treatments and the effect of the nature of the material; (ii) to see if another  
15 protocol could give an equivalent cracking to that obtained after the normalized thermal treatment.  
16 To do so, and because the microstructure has a great influence on the crack pattern (Nasseri *et al.*,  
17 2009), three materials were used: a natural one, Tuffeau limestone, used in traditional or historical  
18 buildings, and two concretes with different aggregates, siliceous and calcareous. According to Xing  
19 *et al.* (2011) and Calmeiro Dos Santos and Rodrigues (2016), the nature of the aggregates will  
20 significantly affect the behavior of concrete after exposure to fire. Their studies indicated that the  
21 strength of calcareous concrete was more affected under 400°C and that above this threshold, the  
22 siliceous aggregate should be the most affected. The applications of the present study are twofold:  
23 to contribute to knowledge of the fundamental mechanics of crack network descriptions and to the  
24 applied engineering issue of understanding the effect of fire on building materials and more  
25 generally the effects of thermal variation.

## 28 2. Methodology

### 30 2.1. Materials

31  
32 Three different materials were selected (see Table 1). They present different properties and  
33 microstructures (Figure 1). Between three to five samples per material were used for each initial  
34 characterization.

35  
36  
37 *Table 1. Materials' initial properties.*

Material	Mass (Kg/m <sup>3</sup> )	Porosity (%)	V <sub>P</sub> (m/s)	V <sub>S</sub> (m/s)	structure
Siliceous Concrete (SC)	2450	11.1	3450	1650	Cohesive matrix
Calcareous Concrete (CC)	2460	11.5	3500	1400	Cohesive matrix
Tuffeau	1360	46.4	1900	1250	Granular

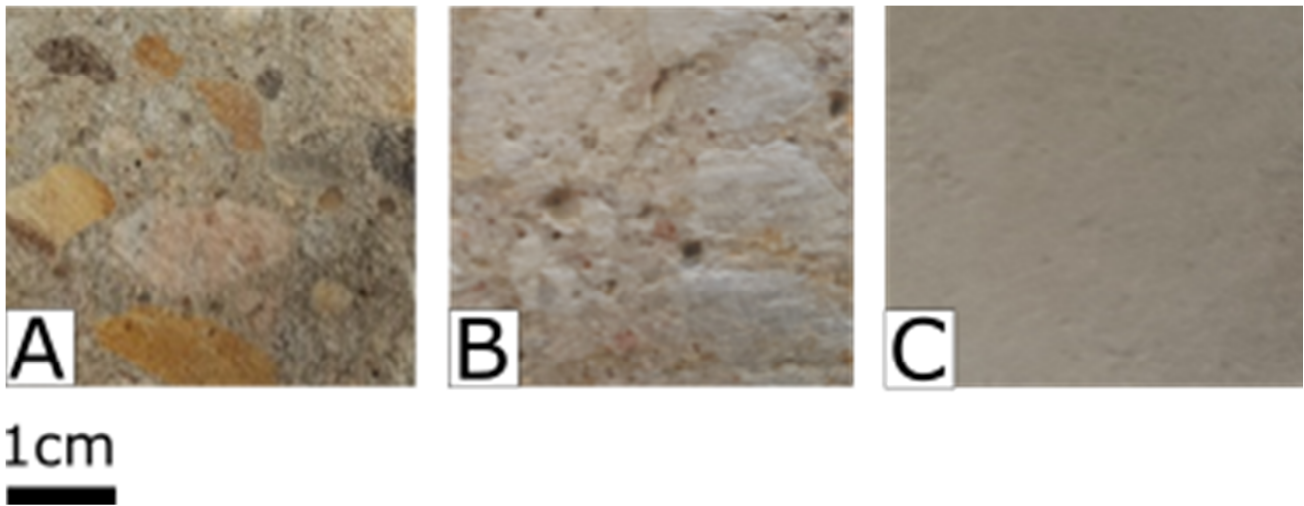


Figure 1. Picture of a) siliceous concrete b) calcareous concrete and b) Tuffeau limestone. Scale bar is indicated for the three pictures.

The first two samples are a siliceous and a calcareous concrete, both prepared in the laboratory from siliceous or calcareous aggregates (about 0/6 size). The water cement ratio is about 0.5. The microstructure is characterized by a cohesive matrix (cement paste) to which sand grains and the corresponding aggregates were drowned. Ordinary Portland cement (OPC), CEM I 52.5 N was used. No superplasticizer or additive was used. Table 2 gives the composition of the obtained two concretes. The initial porosity was low in both cases, about 11%.

Heating/cooling tests were performed after 28 days for the concrete. Samples were placed in water in a curing room at 20 °C.

Table 2. Concrete composition.

Compound	Siliceous concrete (Kg/m <sup>3</sup> )	Calcareous concrete (Kg/m <sup>3</sup> )
CEM I 52.5 N	400	400
Siliceous aggregates	990	-
Calcareous aggregates	-	990
Sand	768	768
Water	195	195

The second material is a natural limestone. Tuffeau is a commonly used stone for traditional and historical buildings in the Loire region. It is made of 50% calcite, 10% quartz, 30% Opal CT and 10% of clay minerals and micas (Beck *et al.*, 2016), and is naturally very porous. Our samples had an initial porosity of 46%.

Table 3 summarizes the samples collected in the different material blocks together with the thermal treatments applied and the measurements performed.

1 Table 3. Samples, thermal treatment and measurements. ETh conductivity stands for the measurement of the effective thermal  
 2 conductivity. HT stands for the High Temperature treatment

Material	n°	Thermal treatment	Measurements
Siliceous concrete	1	Control sample	V <sub>P</sub> , V <sub>S</sub> , porosity, ETh conductivity, microstructural observation (only large scale)
	2	Shock at 70°C	V <sub>P</sub> , V <sub>S</sub> , porosity, ETh conductivity
	3	Shock at 105°C	V <sub>P</sub> , V <sub>S</sub> , porosity, ETh conductivity
	4	Shock at 200°C	V <sub>P</sub> , V <sub>S</sub> , porosity, ETh conductivity
	5	Shock at 800°C	V <sub>P</sub> , V <sub>S</sub> , porosity
	6	HT	V <sub>P</sub> , V <sub>S</sub> , porosity, ETh conductivity, microstructural observation
	7	10 cycles at 180°C	V <sub>P</sub> , V <sub>S</sub> , porosity, ETh conductivity
	8	20 cycles at 180°C	V <sub>P</sub> , V <sub>S</sub> , porosity, ETh conductivity
	9	30 cycles at 180°C	V <sub>P</sub> , V <sub>S</sub> , porosity, ETh conductivity
Calcareous concrete	10	Control sample	V <sub>P</sub> , V <sub>S</sub> , porosity, ETh conductivity, microstructural observation (only large scale)
	11	Shock at 70°C	V <sub>P</sub> , V <sub>S</sub> , porosity, ETh conductivity
	12	Shock at 105°C	V <sub>P</sub> , V <sub>S</sub> , porosity, ETh conductivity
	13	Shock at 200°C	V <sub>P</sub> , V <sub>S</sub> , porosity, ETh conductivity
	14	Shock at 800°C	V <sub>P</sub> , V <sub>S</sub> , porosity
	15	HT	V <sub>P</sub> , V <sub>S</sub> , porosity, ETh conductivity, microstructural observation
	16	10 cycles at 180°C	V <sub>P</sub> , V <sub>S</sub> , porosity, ETh conductivity
	17	20 cycles at 180°C	V <sub>P</sub> , V <sub>S</sub> , porosity, ETh conductivity
	18	30 cycles at 180°C	V <sub>P</sub> , V <sub>S</sub> , porosity, ETh conductivity
Tuffeau	19	Control sample	V <sub>P</sub> , V <sub>S</sub> , porosity, ETh conductivity, microstructural observation (only large scale)
	20	Shock at 70°C	V <sub>P</sub> , V <sub>S</sub> , porosity, ETh conductivity
	21	Shock at 105°C	V <sub>P</sub> , V <sub>S</sub> , porosity, ETh conductivity
	22	Shock at 200°C	V <sub>P</sub> , V <sub>S</sub> , porosity, ETh conductivity
	23	Shock at 800°C	V <sub>P</sub> , V <sub>S</sub> , porosity
	24	HT	V <sub>P</sub> , V <sub>S</sub> , porosity, ETh conductivity, microstructural observation (only large scale)
	25	10 cycles at 180°C	V <sub>P</sub> , V <sub>S</sub> , porosity, ETh conductivity
	26	20 cycles at 180°C	V <sub>P</sub> , V <sub>S</sub> , porosity, ETh conductivity
	27	30 cycles at 180°C	V <sub>P</sub> , V <sub>S</sub> , porosity, ETh conductivity

## 2.2. Thermal protocols

3  
 4  
 5  
 6 Three protocols were applied (see Figure 2) in order to reproduce the high temperature conditions  
 7 of fire, the rapid cooling and the seasonal variations. Note that in all these protocols, no  
 8 thermocouples were used; the thermal variations are monitored by the oven capacities.  
 9  
 10  
 11  
 12  
 13

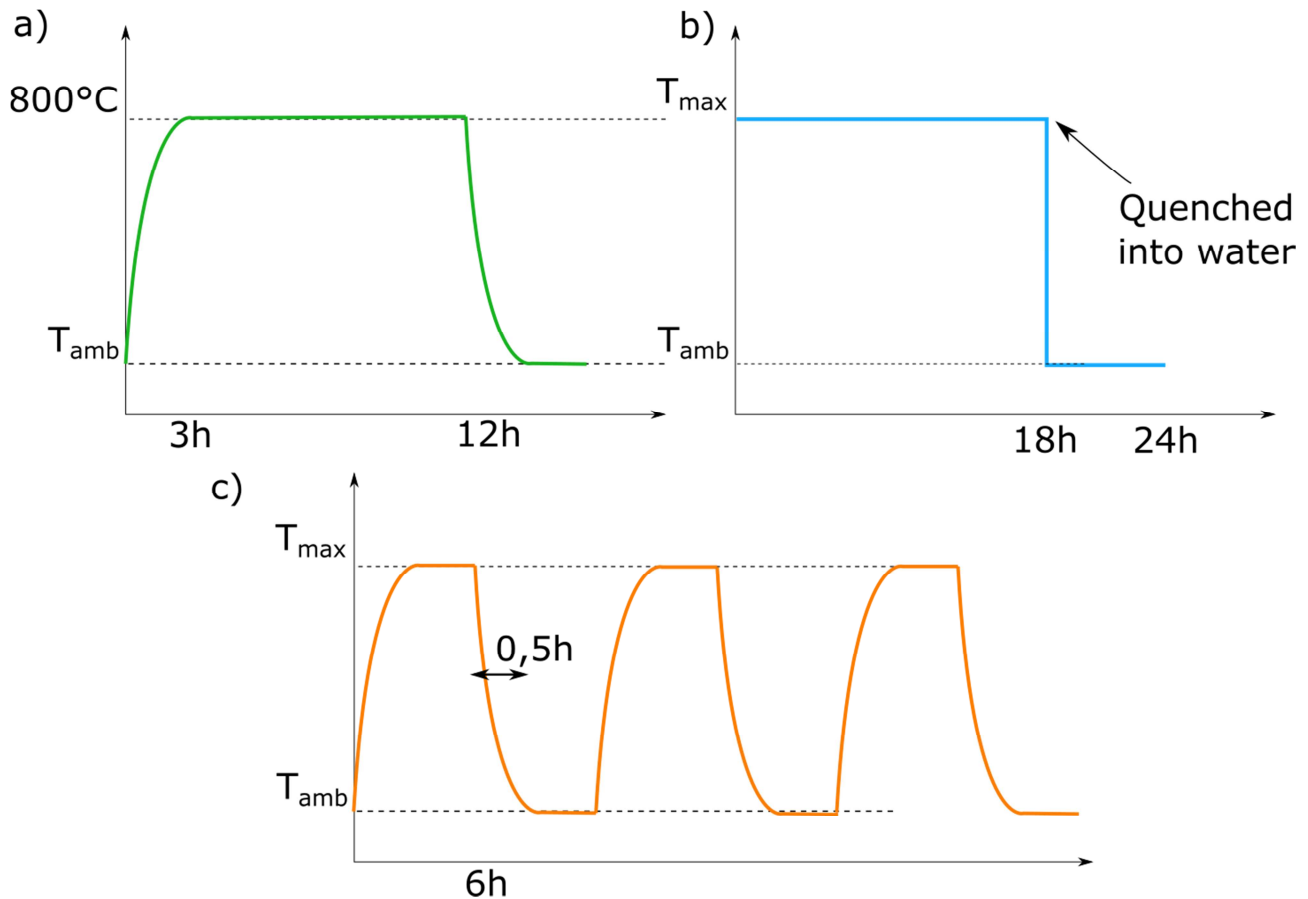


Figure 2. The three thermal protocols. a) High temperature test, where samples are heated up to  $800^{\circ}\text{C}$  and progressively cooled. b) Thermal shock, where samples are heated up to  $T_{max}$  (70, 105, 200  $800^{\circ}\text{C}$ ) and then quenched in water. c) Thermal cycling, where samples are slowly heated up to  $180^{\circ}\text{C}$  and cooled in a number of cycles (10, 20 and 30 cycles).

**High Temperature treatment (HT)** was performed following the normalized procedure to study the material resistance to fire. The normalized procedure follows a particular temperature curve (ISO834-1999) in which samples are slowly heated following a logarithmic temperature increase, firstly up to  $800^{\circ}\text{C}$  and then up to  $1110^{\circ}\text{C}$ . As we did not have at our disposal an oven able to reach this second level, our HT treatment was slightly different from the normalized test (Figure 2a): the temperature slowly reached  $800^{\circ}\text{C}$  in 3h. This is due to our high temperature furnace limitations (about  $900^{\circ}\text{C}$  with a heating rate of  $4^{\circ}\text{C}/\text{min}$  and an accuracy of  $\pm 1^{\circ}\text{C}$ ). After reaching this temperature, samples were held at this level for 12h in order to ensure a homogeneous temperature diffusion up to the sample core (recently discussed by Zhang *et al.*, 2018). Then, the temperature was progressively cooled down. This high temperature oven is not equipped with a cooling control, but the temperature decrease was measured and found to be slow, at around  $1^{\circ}\text{C}/\text{min}$ . Even if the protocol is slightly different from the standard one, the principle of thermal treatment is the same: a high temperature and slow heating and cooling, and can thus be expected not to have a significant impact on the mechanical results. This thermal treatment was therefore considered as our normalized fire procedure. Due to the limited availability of this oven in our laboratory and its complexity of use, it was used only for this treatment.

**The thermal shocks** were performed with a simple oven in which the heating rate is fixed at  $1^{\circ}\text{C}/\text{min}$ . Three maximum temperatures were applied (Figure 2b): 70, 105 and  $200^{\circ}\text{C}$ . Higher temperatures were not possible due to oven limitations. The temperature was maintained for 12 h in order to ensure a constant temperature up to the sample core as in the previous procedure. Then, the samples were quenched in water (Mallet *et al.*, 2013, 2014) and remained in the water for 6 h until

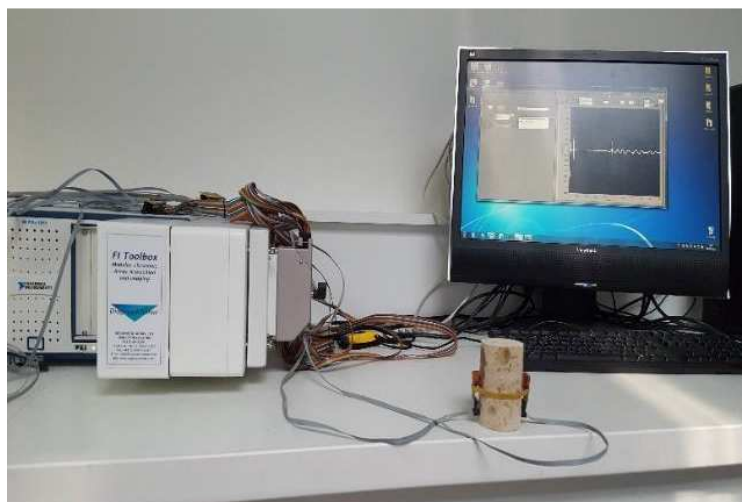
1 total cooling (NF-EN14066). They were then oven-dried and placed in a desiccator. The rock mass  
2 evolution was monitored to ensure that complete drying was achieved. As the influence of the  
3 cooling process is an important parameter that affects the mechanical properties and the crack  
4 network (Botte and Caspeepe, 2017), a fourth thermal shock was applied. Each sample put in the HT  
5 oven was duplicated and one of the two was quenched in water after the 12 h at 800°C. This  
6 thermal shock at such a high temperature was performed in order to examine the effect of cooling  
7 rate.

8  
9 **Thermal cycle** is a repetitive protocol (Figure 2c). Samples were placed in an oven that was  
10 progressively heated up to 180°C in 30 min and then cooled after 6 h down to 20°C in 30 min.  
11 These progressive 7-hour cycles were repeated 10, 20 and 30 times (Yavuz *et al.*, 2006; Lam Dos  
12 Santos *et al.*, 2011). It is commonly considered in the literature that this protocol leads to  
13 homogeneously damaged samples due to its progressive aspect (Wang et al., 2013). A perfectly  
14 controlled oven was used that allows temperature regulation from -60°C to 200°C with a precision  
15 of 0.1°C. This furnace can be programmed for automatic cycles.

16  
17 After all the thermal treatments, the samples were preserved in an oven with controlled humidity  
18 (dry, Hr=40%) and temperature (45°C).

### 20 2.3. Measurements

21  
22 **Elastic wave velocities** were measured with piezoelectric sensors (PI Ceramic). The sensors were  
23 placed directly on the sample surface and maintained thanks to rubber bands (Figure 3). Honey was  
24 used as couplant in order to ensure a good contact between the sensor and the sample. Two sensors  
25 were placed on opposite faces of the sample in the radial direction of the cylinder. The  
26 measurement principle is as follows: an electric pulse of 150 V is generated and transmitted to the  
27 first sensor. It triggers a mechanical vibration that propagates into the sample. This wave has a  
28 resonant frequency of 150 kHz. The opposite sensor records this vibration and transforms it into an  
29 electrical signal that is amplified at 30 dB. The signal is recorded and observed on a dedicated  
30 interface (Figure 3). Finally, the travel time of the elastic pulse through the sample is manually  
31 picked. Knowing the distance between the two sensors, the elastic wave velocity can be determined  
32 (Birch, 1960). We used compressional (P) and shear (S) wave sensors to obtain the P- and S-wave  
33 velocities.



35  
36  
37 *Figure 3. Elastic wave velocity measurement assembly, with the generator (on the left), the sample and two opposite sensors, and the view of the dedicated interface for the wave observations (on the right).*

1 The elastic wave velocities were determined with an accuracy of  $\pm 50$  m/s. Note that this measurement  
 2 accuracy is due to the travel time picking and the signal sampling. The elastic modulus can be obtained  
 3 from these velocities considering a simple isotropic symmetry by:

$$V_p^2 = \frac{K + \frac{4}{3}G}{\rho} \quad \text{and} \quad V_s^2 = \frac{G}{\rho},$$

4 where  $K$  and  $G$  are the bulk and shear modulus, respectively, and  $\rho$  is the sample density. The  
 5 sample density was measured by weighing the samples before the thermal treatments. The densities  
 6 are given in Table 1.

7  
 8 **Crack density** is a mechanical damage parameter introduced by Walsh (1965a, b) in order to  
 9 quantify the effect of cracks on the elastic properties. In scalar definition and the isotropic case, it is  
 10 defined by the ratio of the sum of all cubed crack radii versus the total volume of the sample:

$$\rho_c = \frac{1}{V_T} \sum_i a_i^3,$$

11 where  $a_i$  is the radius of the  $i^{\text{th}}$  crack and  $V_T$  is the total volume of the sample. Then, still  
 12 considering the simple isotropic case, the crack density can be linked to elastic parameters (and thus  
 13 elastic wave velocities) by the following relationships derived from the study by Kachanov (1993):

$$\frac{K_0}{K} = 1 + \rho_c \frac{16(1 - \nu_0^2)}{1 - 2\nu_0}$$

14 and

$$\frac{G_0}{G} = 1 + \rho_c \frac{16(1 - \nu_0/5)(1 - \nu_0)}{9(1 - \nu_0/2)}$$

15 where the subscript 0 refer to the initial sample (without cracking), and  $\nu_0$  is the Poisson's ratio.

16  
 17 **Effective Thermal conductivity** was measured in order to describe the crack connectivity. As  
 18 shown by Xiong and Liew (2016), thermal or electrical conductivities are linked to the connectivity  
 19 of a crack network. When a sample is more porous, its effective thermal conductivity decreases.  
 20 Thus, when cracks are more numerous and connected, a decrease in conductivity can be expected.  
 21 This measurement was performed by the hotwire technique following ASTM D5930-97 and the  
 22 RILEM recommendation (AAC11-3). The Neotim apparatus used is equipped with a probe of  
 23 50 mm in length. The accuracy of the measurement is  $\pm 5\%$  with a repeat accuracy of 3%. The  
 24 temperature range of the apparatus is from  $-20^\circ\text{C}$  to  $100^\circ\text{C}$ . The measurement range of effective  
 25 thermal conductivity was 0.02 to 5 W/mK. For every measurement, the average conductivity was  
 26 obtained from 10 measurements in order to minimize the standard deviation.

27  
 28 Lastly, **Porosity** was measured, thanks to water saturation. It is only the water accessible porosity.  
 29 To do so, the sample mass has been measured and thus, the density could be follow. However, these  
 30 results are not presented here. They do not show discussable tendency as in the high temperature  
 31 investigation performed by Motra and Zertani (2018). We also performed some **microstructural**  
 32 **observations** under an optical microscope for qualitative descriptions.

### 35 3. Results

#### 36 3.1. Elastic wave velocity and crack density

37  
 38  
 39 Figure 4 presents the P-wave (in blue) and S-wave (in orange) velocities measured after  
 40 the different thermal treatments. Figures 4a and b concern the siliceous and calcareous concretes,

1 respectively, while Figure 4c concerns the Tuffeau limestone. The velocities measured on the initial  
2 samples are represented as an empty circle. Results obtained after thermal shocks are plotted as  
3 stars; after the thermal cycles, as squares (with an exponent corresponding to the number of cycles);  
4 and after the HT treatment, as a filled circle. Note that for the S-wave, it is not easy to distinguish  
5 the squares, but for every case, the results for the 10-cycle protocol are the highest velocities and  
6 those with 30 cycles are the lowest.

7 Increasing the maximum temperature of the thermal shock decreased the elastic velocities, although  
8 this is not very marked for the first three values of the Tuffeau limestone, as considering the error  
9 bar of the elastic wave measurements ( $\pm 50$  m/s), a thermal shock of 70 or 105°C appeared to lead to  
10 no velocity variations in this material compared to the initial state. In contrast, we always observed  
11 a variation with the increasing number of cycles, whatever the sample. Concerning the high  
12 temperature treatment, we can see that for the S-wave, the velocity reached is equivalent to the one  
13 obtained after a thermal shock at 800°C. For the calcareous materials (calcareous concrete and  
14 Tuffeau), the velocities measured after the HT treatment presented the biggest difference with the  
15 initial state. This was not the case for the siliceous concrete where the thermal shock at 800°C led to  
16 even lower velocities than with the high temperature treatment. In order to interpret the cracking  
17 behavior in greater detail, we now focus on the crack density inferred from both P- and S-wave  
18 velocities.

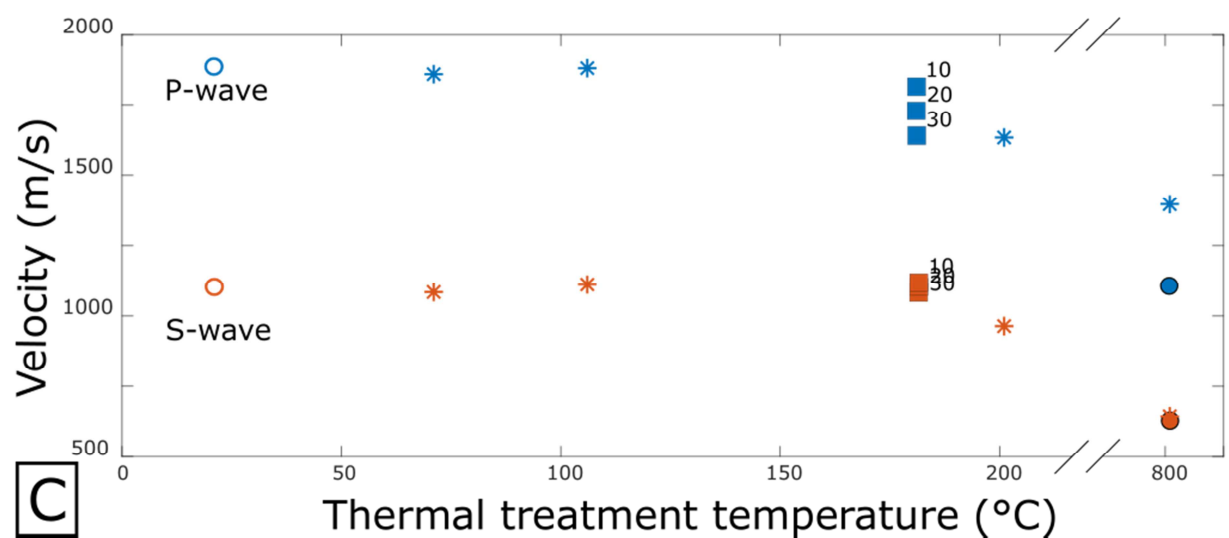
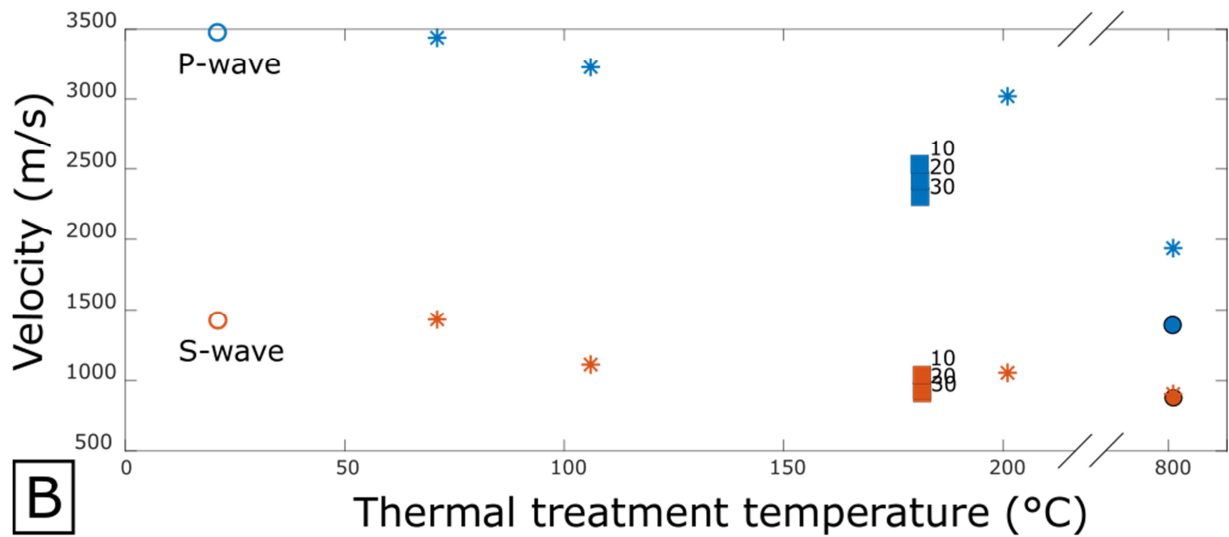
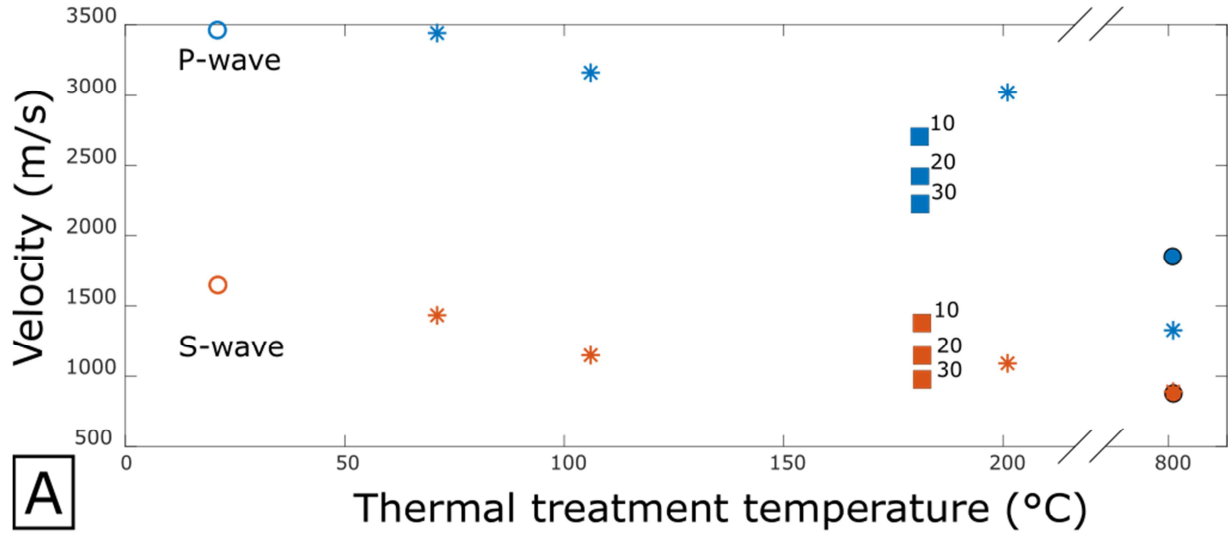
19  
20 In Figure 5, the crack density is plotted with the same symbols as previously. Here also, Figures 5a  
21 and b concern the siliceous and calcareous concretes, respectively, while Figure 5c concerns the  
22 Tuffeau. Because it is known that crack density describes the mechanical damage due to cracks, this  
23 Figure can be directly interpreted in terms of sample cracking. For the two calcareous samples (the  
24 calcareous concrete and the Tuffeau), the maximum crack density was obtained after the high  
25 temperature treatment, and the result obtained with the thermal shock performed at 800°C was the  
26 closest to the HT results. For the siliceous concrete, it was the thermal shock at 800°C that caused  
27 the most damage, and the result obtained after 30 cycles was the closest to the HT results. This  
28 material appears to be much more affected by a sharp high temperature decrease than the calcareous  
29 concrete, as expected according to the study by Calmeiro Dos Santos and Rodrigues (2016).

30  
31  
32 These results on thermal shock and repetitive cycles show that the concrete and Tuffeau samples do  
33 not have the same behavior.

34 For the concretes, the slightest thermal shock immediately favors an increase in crack density. This  
35 is not the case for Tuffeau where the first two thermal shocks present the same crack density as the  
36 initial state (i.e.  $\rho_C = 0$ ). For the concretes, the increasing number of cycles has a strong effect on  
37 the crack density (particularly for the siliceous concrete) as can be seen from the great difference  
38 between 10, 20 and 30 cycles, with crack density going from 0.2 to 0.8 for the siliceous concrete  
39 and from 0.45 to 0.8 for the calcareous concrete. The repetitive cycles at 180°C strongly affect the  
40 damage. Crack density is greater at lower temperature after 20 cycles. In addition, the cracking  
41 obtained after 30 cycles is close to the crack density induced by the high temperature treatment (at  
42 least compared to the result obtained on Tuffeau, and especially for the siliceous concrete).

43 The behavior of Tuffeau is different. The first shocks do not induce a marked increase in cracking  
44 damage since for thermal shocks up to 105°C, the crack density is almost zero. It presents a slight  
45 increase, but this is negligible considering the error bar on the elastic wave velocities (leading to a  
46 crack density known with an accuracy of  $\pm 0.005$  determined by Mallet *et al.*, 2013). The increasing  
47 damage due to the heating-cooling cycles is less than for the concrete. The first two thermal shocks  
48 do not induce a damage increase compared to the initial state. Moreover, unlike the concrete, the  
49 thermal shock at 200°C is the most damaging. This difference no doubt comes from the  
50 microstructure of the sample, studied in the following section.

1



2

3

4

5

6

7

Figure 4. P- and S- wave velocities obtained a) for the siliceous concrete, b) for the calcareous concrete and c) for the Tuffeau. Blue dots are P-waves, orange dots are S-waves. The empty circle is the initial state, stars are the measurements obtained after thermal shocks, the squares are after the successive cycles and the filled circle is the measurement obtained after the high temperature treatment. For each point, the error bar is about  $\pm 50$  m/s which is approximately the dot size.

8

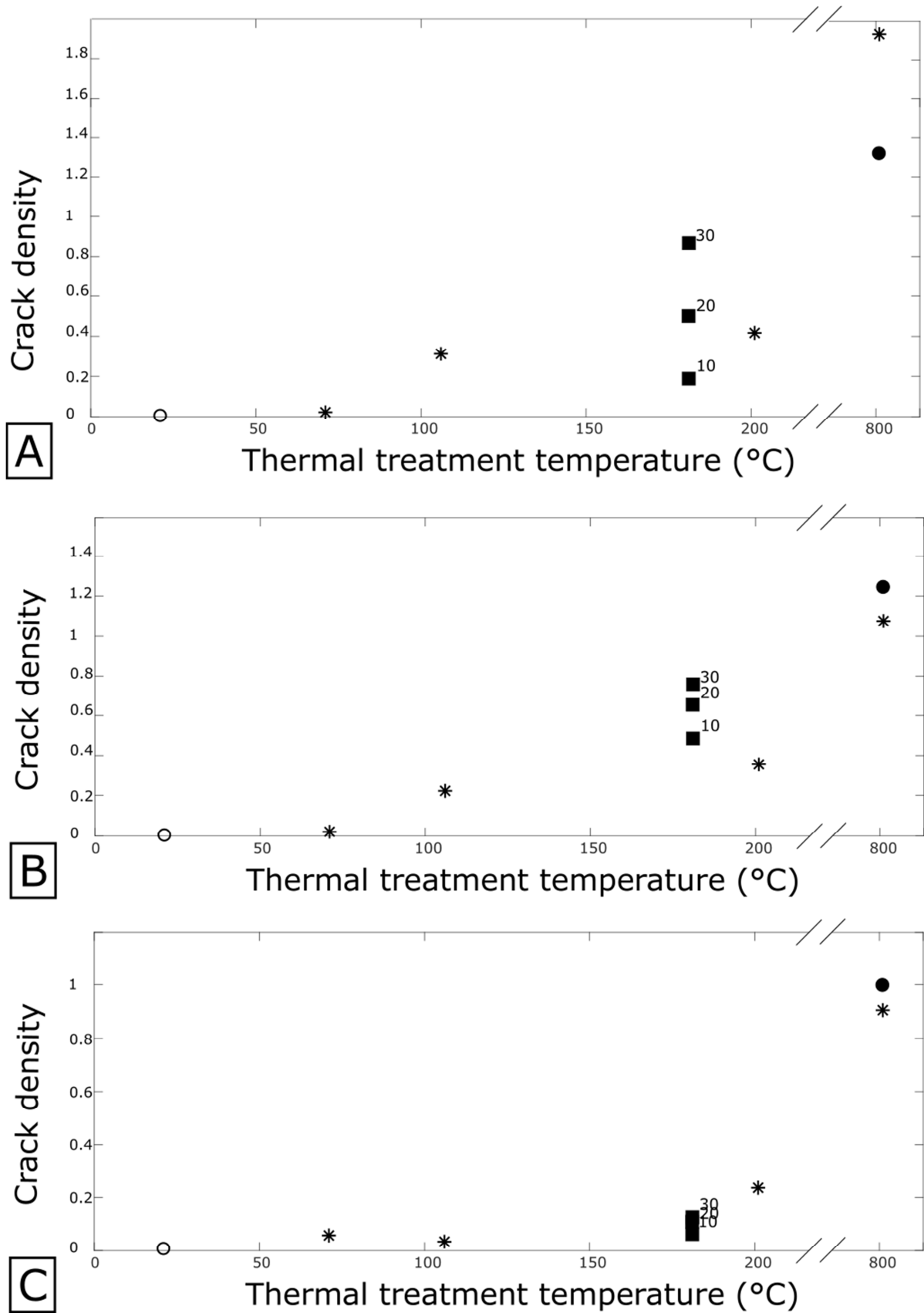


Figure 5. Crack densities obtained in a) the siliceous concrete, b) the calcareous concrete and c) the Tuffeau. As for Figure 4, the empty circle is the initial state, the stars are the measurements obtained after thermal shocks, the squares are after the successive cycles and the filled circle is the measurement obtained after the high temperature treatment. Due to the velocity errors, the crack densities are known with an accuracy of  $\pm 0.005$  (Mallet et al. 2013).

1  
2  
3  
4  
5  
6

### 3.2. Porosity and effective thermal conductivity

Figures 6 and 7 show the effective thermal conductivity and porosity versus the crack density results obtained after the different thermal solicitations. The symbols are the same as for Figures 4 and 5.

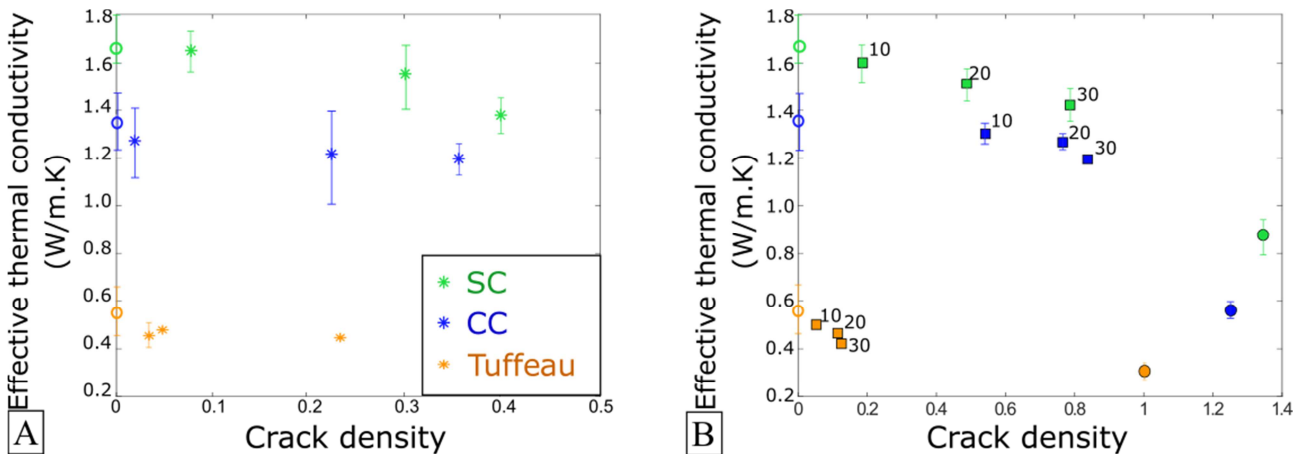


Figure 6. Effective thermal conductivity evolution with crack density. Green dots are for siliceous concrete (SC) blue dots are for calcareous concrete (CC) and orange dots are for the Tuffeau. On both figures and as for Figure 4, the empty circle is the initial state, the stars are the measurements obtained after thermal shocks (a), the squares are after the successive cycles and the filled circle is the measurement obtained after the high temperature treatment (b). Effective thermal conductivity is known with an accuracy of 5%. Larger discrepancies are shown with vertical bars.

The effective thermal conductivity is a good indicator to monitor the damage evolution, especially the fluid flow capacity as it is a sign of crack connectivity (Han *et al.*, 2015; Xiong and Liew, 2016). When a material is cracked, if the network is fully connected, the air tunnels will block thermal diffusion. Thus, a decrease in effective thermal conductivity is expected when the crack connectivity increases. In civil engineering, thermal or electrical conductivity is also considered in order to assess cracking in buildings (Lataste *et al.*, 2003). In the present study, the effective thermal conductivity was compared to the initial value of the non-damaged material in order to determine the relative variation of the global connectivity of the crack network. It is, however, not our purpose to propose a quantitative measurement of this property.

We observe that for the three materials, when crack density increases, effective thermal conductivity decreases. This decrease is much more pronounced for the concretes and for the repetitive cycling protocols. Looking in greater detail, the calcareous concrete appears to have a different behavior from the siliceous concrete: the discrepancy between the measurements of the two concretes is larger than for the measurements performed after the thermal shocks (Figure 6a). Finally, we observe a strong decrease, again especially for the concretes, between the low temperature treatment and the treatment at 800°C. Note that the sample submitted to the thermal shock performed at 800°C could not be measured due to its lack of integrity.

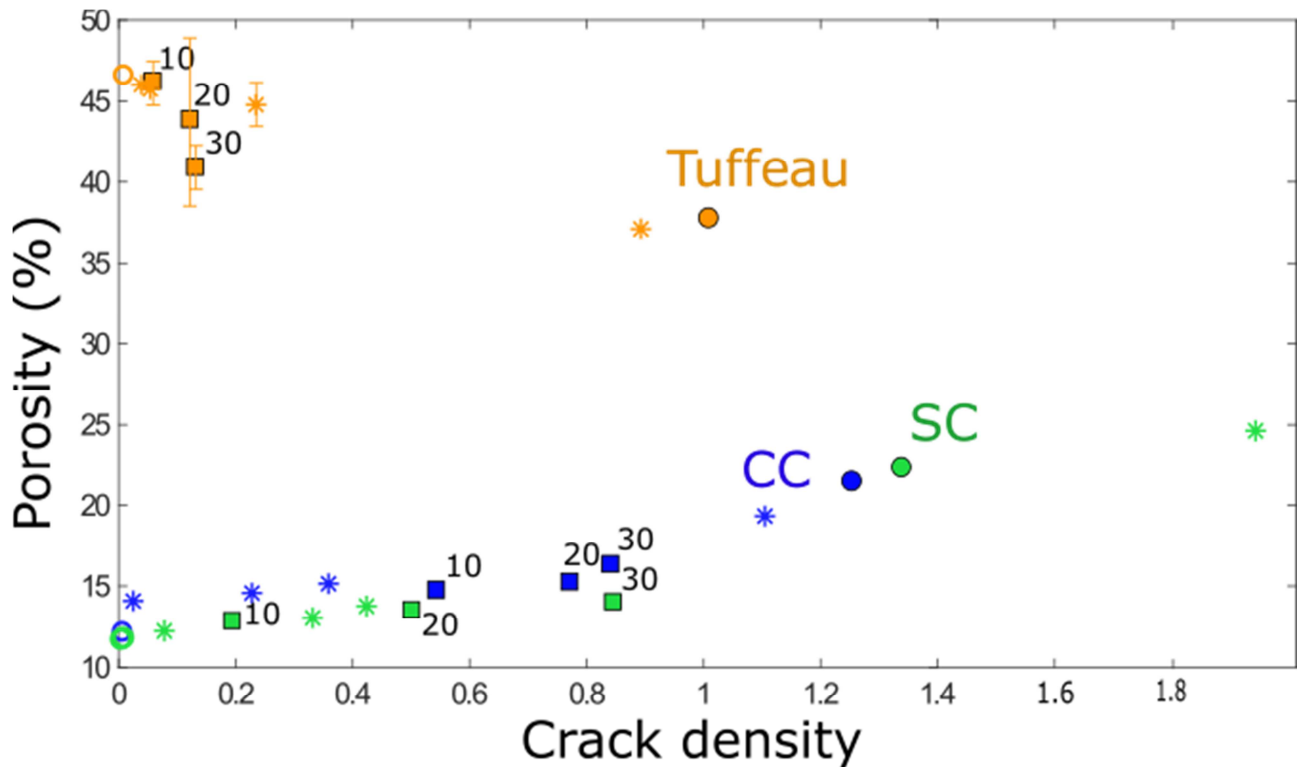


Figure 7. Porosity evolution with crack density. The same symbols are used as in Figure 6. When the discrepancy for the porosity measurement was larger than 2% (the dot size) it has been added on the Figure.

Figure 7 represents the evolution of the measured porosity with the crack density. Two behaviors can be clearly observed: for the concretes, which have a similar behavior whatever the aggregate, when crack density increases, the global porosity increases. This result is unsurprising. An opposite trend is observed for the Tuffeau, although there are some discrepancies in the results. The increase in crack density is not followed by a porosity increase. This result is not intuitive and will be discussed below.

## 4. Discussion

### 4.1. Materials comparison and interpretation in terms of crack network

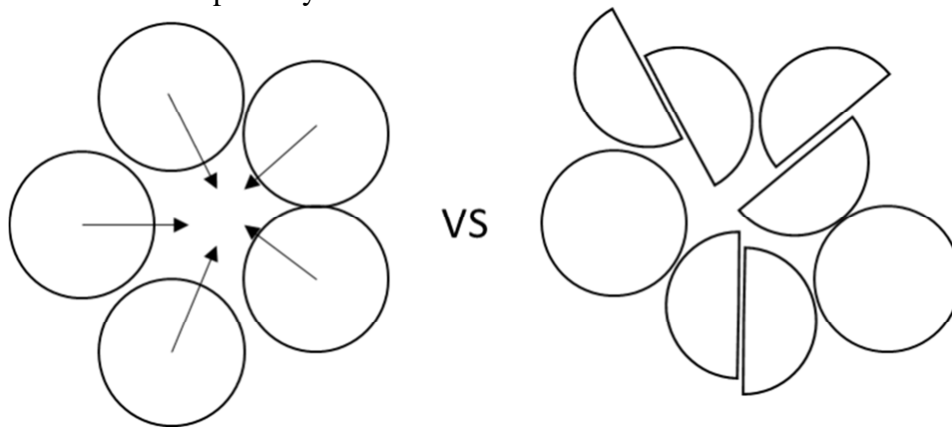
The two concretes respond to the different thermal stresses in the same manner as many other geomaterials. The increase in crack density with thermal shock has been widely observed in non-crystalline materials that could represent the behavior of the concrete matrix (Mallet et al., 2013, 2014) but also in granite (Liu *et al.*, 2018) that presents an equivalent microstructure of grain variation. With the increasing number of cycles, the crack network is much denser and more connected, which was also observed in Westerly granite (Liu *et al.*, 2018). In the latter study, the authors presented an experimentally validated mathematical model based on fracture mechanics and thermo-elasticity to describe how transport properties, or in our case, effective thermal conductivity, changes with a higher thermal stress. Their results indicated that thermal cracking is mainly driven by the difference between mineral thermal expansion coefficients. This explains our observation for the concrete: even if the temperature increases slowly, when thermal treatment increases, grains dilate, and because of the cemented matrix, cracks are nucleated. These same differences observed

1 for the studied materials have been explained in the literature (see for example Ingham 2009 and  
2 Zhang et al. 2017).

3 The difference between the two concretes could be explained by the different strength of the two  
4 aggregates. In the high temperature treatment, the difference could also come from the alpha-beta  
5 quartz transition observed after 575°C that can occur in siliceous concrete (Shapiro *et al.*, 1967;  
6 Carpenter *et al.*, 1998). This well-known phenomenon which produces structural changes may  
7 cause changes in volume and differential cracking that is even observed in amorphous materials  
8 (Chakrabarti *et al.*, 1995).

9

10 For the Tuffeau, there is no damage at the beginning of the thermal treatments. This is similar to  
11 what is observed in many different limestones or sandstones, and can be explained by the calcite  
12 matrix and the high porosity which allow the grains to dilate unhindered. It could also be an  
13 explanation for the non-intuitive porosity variation of the Tuffeau. Because of the high initial  
14 porosity (46%), when the samples are heated, grains can dilate, decreasing the void between them  
15 as observed in the study by Bachrach *et al.* (2000). On the other hand, it must be borne in mind that  
16 we are measuring water porosity. It is possible that the apertures in the created cracks are too small  
17 for water to penetrate. It has been shown in porous sandstones that two mechanisms can occur  
18 (Fortin *et al.*, 2009): grains can “leave” their original place and “fall” into the pores, or small  
19 microcracks can be created inside grains (Figure 8), leading in both cases to a pore collapse and a  
20 decrease in water-accessible porosity.



21

22

23

Figure 8. Schematic illustration of porosity decrease in granular and porous material versus microcracks developing at the grain scale (adapted from Fortin *et al.*, 2009).

24

25

#### 4.2. Effect of the different thermal treatments

26

27 As previously mentioned, one of the goals of this study was to show the possibility of using a  
28 simple test to replace the normalized fire test. The comparison presented above shows however that  
29 the three materials do not present the same behavior with respect to the used protocols. The nature  
30 of the material has therefore to be considered in order to describe an equivalent protocol to the  
31 normalized one.

32

33 For the calcareous concrete, the repetitive thermal cycles are more damaging than the thermal  
34 shocks. Comparing the crack density gap between 30 cycles and the HT protocol result, an  
35 equivalent protocol to the normalized one could simply consist in increasing the number of cycles  
36 with a smaller temperature. However, the different behavior between the shocks and the heating-  
37 cooling cycles observed with the effective thermal conductivity indicates that the cracks induced by  
38 these two stresses do not present the same connectivity. When trying to adapt the normalized  
39 protocol, the cooling rate needs to be especially studied.

40

1 For the siliceous concrete, the sample appears to be much more sensitive to sharp thermal  
2 variations. Nevertheless, as for the calcareous concrete, at lower temperature, the repetitive cycles  
3 give very similar results to those of the HT treatment. One possibility in this case, therefore, would  
4 be to mix these protocols, involving a succession of sharp temperature variations of 200°C,  
5 cyclically repeated. Alternatively, perhaps a single thermal shock at an intermediate temperature  
6 around 400°C would be enough.

7  
8 For Tuffeau it is much more complicated to propose an equivalent protocol as none of the thermal  
9 treatments give similar results to those of the HT treatment. It seems that for this material it is not  
10 possible to find an equivalent test because of its complex fire behavior.

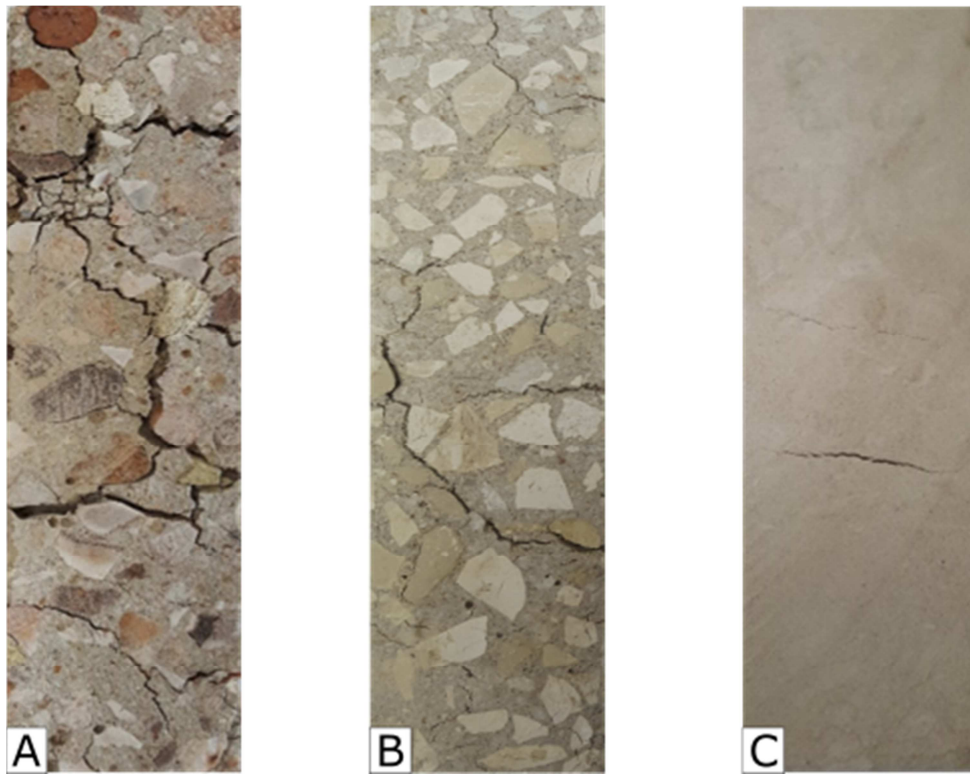
### 11 **4.3. Limitations of our interpretations**

12  
13  
14  
15 We interpreted the observed damage evolution and the property variations by considering cracking,  
16 assessed by the variation in crack density and, as we will see, by some microstructural observations.  
17 However, we are aware that complementary effects could arise, such as a decarbonation reaction for  
18 the calcareous samples treated at 800°C. It has been shown that in the presence of calcite, some  
19 decarbonation reactions coupled to microcracking significantly reduce the rock strength (see for  
20 example the studies by Mollo *et al.*, 2013 and Heap *et al.*, 2013). In addition, some chemical  
21 reactions may occur when the concrete is quenched in water. These other mechanisms may also be  
22 part of the global process, but were beyond the scope of this paper.

23  
24 There is another limitation of our interpretation linked to the use of the crack density parameter.  
25 Thanks to the numerical studies by Grechka and Kachanov (2006) and the experimental study by  
26 Mallet *et al.* (2014), an empirical threshold of around 0.25 can be fixed for the use of this  
27 parameter. This does not mean that beyond this value we cannot calculate the crack density, but the  
28 mechanical interpretation based on the effective medium theories are no longer valid. In this paper,  
29 because our interpretations are based both on the elastic wave velocities and the crack density, we  
30 chose to keep the observation of the variation in crack density. It should be borne in mind, however,  
31 that its exact value is questionable after the above-mentioned threshold. Moreover, concerning  
32 Tuffeau, its high initial porosity will affect the determination of the crack density. However, here  
33 again, because we are comparing the initial state versus the damaged one, we are not looking for an  
34 exact value, but rather a relative behavior. Indeed, following the studies of Schöpfer *et al.* (2009)  
35 and Panza *et al.* (2019) relative crack density can still be investigated even for samples with an  
36 initial high porosity.

### 37 38 **4.4. Microstructural observations**

39  
40  
41 The global microstructure of the Tuffeau and the concretes was observed in the initial state and after  
42 the HT treatment (Figure 9). Note that we are only interested here in providing a qualitative  
43 description. Thus no SEM images were produced. Despite the crack nucleation in the other thermal  
44 treatments, the cracks were visible with the naked eye only for the HT process. We therefore  
45 confined our observations to these samples.



1  
2  
3  
4  
5  
6  
7  
8  
9  
10  
11  
12  
13  
14  
15  
16  
17  
18  
19  
20  
21  
22  
23  
24

Figure 9. Pictures of the samples subjected to the high thermal treatment: a) siliceous concrete, b) calcareous concrete, c) Tuffeau. Pictures are of the whole prismatic samples of 16/4 cm.

The Tuffeau presents only a few large cracks at the surface. The others are small and difficult to observe due to their narrowness. This observation confirms the interpretation of the small aperture blocking water penetration during the porosity measurement. While this could imply that the quality of the measured porosity is not good enough, it is still an interesting result because it provides information about the crack aperture size (about water size) and the interpreted micro-cracking process. We have just to keep in mind that it is not the real porosity but only the water accessible porosity. For future investigations, a mercury porosity measurement would be more accurate.

For the same thermal treatment, the two concretes present a different crack network. The cracks are much more numerous and larger than in the Tuffeau, enabling us to perform much more accurate observations under the optical microscope. On the siliceous concrete, we observed the presence of two crack families that developed around and inside grains (Figure 10a,b). Similar observations are reported in the literature in other granular materials such as the Westerly granite (Nasseri *et al.*, 2009). In the calcareous concrete, this difference was not clearly observable. Only cracks in the matrix and around grains are found (Figure 10c). This could explain the different behavior due to grain strength. Our results are in agreement with those of previous investigations (Xing *et al.*, 2011; Calmeiro Dos Santos and Rodrigues, 2016): at high temperatures, the siliceous-based concrete is more affected and shows many more cracks. However, cracking occurred in the same way for the two concretes at the paste-aggregate interface.

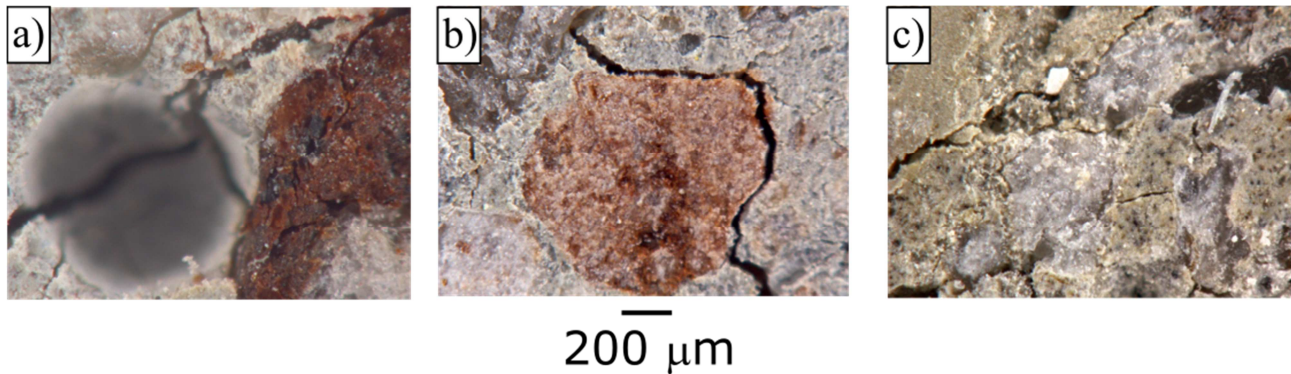


Figure 10. Microstructural observation of cracks in the siliceous concrete (a-b). A crack developed inside a grain (a) and around a grain (b). c) cracks observed in the matrix of the calcareous concrete, around grains. Scale bar is indicated for the three pictures.

## 5. Conclusion

This paper has presented an experimental investigation into the behavior of building materials subjected to thermal variations. Three traditional materials were used, calcareous and siliceous concretes and Tuffeau limestone. Properties related to thermal cracking such as porosity, effective thermal conductivity and wave velocity were examined before and after exposure to temperature variations. Samples were exposed to heating-cooling cycles at 180°C, thermal shocks up to 200°C and high thermal heating according to the ISO834 fire standard.

Based on the results of this study, the following conclusions can be drawn:

- (1) For the concretes, the greatest damage is caused by the normalized high thermal treatment or the thermal shock at 800°C. The closest damage to the HT is obtained with the repetitive thermal cycles.
- (2) Sharp thermal variations have a more significant effect on siliceous concrete than on calcareous concrete. The use of calcareous aggregates could be an effective method to increase the crack resistance of concrete.
- (3) For Tuffeau, the damage observed after the thermal shock at 200°C is the closest to that obtained after the high temperature treatments.
- (4) The porosity of siliceous and calcareous concrete increased with the increase in crack density. The Tuffeau limestone showed an opposite behavior due to grain expansion.
- (5) The crack connectivity after thermal shock and after the repetitive heating-cooling cycles is different: thermal shocks lead to more connected cracks.
- (6) There is no single equivalent protocol to high thermal treatment but rather different protocols depending on the material properties.

## Acknowledgments

The data reported in this work can be obtained from the corresponding author upon request. The authors gratefully acknowledge financial support from PRISME Laboratory.

## References

Al-Omari, A., Brunetaud, X., Beck, K., Al-Mukhtar, M. (2014). Coupled thermal-hygric characterisation of elastic behaviour for soft and porous limestone. *Construction and Building Materials*, **62** 28-37.

Bachrach, R., Dvorkin, J., Nur, A. M. (2000) Seismic velocities and Poisson's ratio of shallow unconsolidated sands. *Geophysics*, **65**(2) 559-564.

- 1 Beck, K., Janvier-Badosa, S., Brunetaud, X., Török, A., Al-Mukhtar, M. (2016). Non-  
2 destructive diagnosis by colorimetry of building stone subjected to high temperatures. *European*  
3 *Journal of Environmental and Civil Engineering*, **20**(6) 643-655.
- 4 Belayachi, N., Hoxha, D., Do, D. P. (2012). Thermo-hydro-mechanical behavior of Tuffeau  
5 stone masonry. *European Journal of Environmental and Civil Engineering*, **16**(5) 557-570.
- 6 Birch, F. (1960). The velocity of compressional waves in rocks to 10 kilobars, part 1. *Journal*  
7 *of Applied Mechanics*, **65** 1083-1102.
- 8 Botte, W., Caspeepe, R. (2017). Post-cooling properties of concrete exposed to fire. *Fire*  
9 *Safety Journal*, **92** 142-150.
- 10 Calmeiro Dos-Santos, C., Rodrigues, J. P. C. (2016). Calcareous and granite aggregate  
11 concretes after fire. *Journal of Building Engineering*, **8** 231-242.
- 12 Carpenter, M. A., Salje, E. K. H., Graeme-Barber, A., Wruck, B., Dove, M. T., Knight, K. S.  
13 (1998). Calibration of excess thermodynamic properties and elastic constant variations associated  
14 with the alpha-beta phase transition in quartz. *American mineralogist*, **83**(1-2) 2-22.
- 15 Chakrabarti, A., Kuhlman, G. W., Rohde, K. A. (1995). High strength titanium aluminium  
16 alloy improved fatigue crack growth resistance. *US Patent* No5,399,212.
- 17 Fortin, J., Stanchits, S., Dresen, G., Guéguen, Y. (2009). Acoustic Emissions Monitoring  
18 during Inelastic Deformation of Porous Sandstone: Comparison of Three Modes of Deformation.  
19 *Pure And Applied Geophysics*, **166** 823-841.
- 20 Ghazi Wakili, K., Hugi, E., Wullschleger, L., Frank, T. (2007). Gypsum board in fire  
21 modeling and experimental validation. *Journal of Fire Sciences*, **25**(3) 267-282.
- 22 Grechka, V. Kachanov, M. (2006). Affective elasticity of fractured rocks: a snapshot of the  
23 work in progress. *Geophysics*, **71**(6) W45-W58.
- 24 Guéguen, Y., Kachanov, M. (2011). Effective elastic properties of cracked rocks - an  
25 overview, in, mechanics of crustal rocks. *CISM Courses and Lectures* **533** 73-125.
- 26 Han, T., Best, A. I., Sothcott, J., North, L. J., MacGregor, L.M. (2015). Relationships among  
27 low frequency (2 hz) electrical resistivity, porosity, clay content and permeability in reservoir  
28 sandstones. *Journal of Applied Geophysics*, **112** 279-289.
- 29 Heap, M. J., Mollo, S., Vinciguerra, S., Lavallée, Y., Hess, K.-U., Dingwell, D., Baud, P.,  
30 Iezzi, G. (2013). Thermal weakening of the carbonate basement under Mt. Etna volcano (Italy):  
31 implications for volcano instability. *Journal of volcanology and geothermal research*, **250** 42-60.
- 32 Hoseini, M., Bindiganavile, V., Banthia, N., (2009). The effect of mechanical stress on  
33 permeability of concrete: a review. *Cement and concrete composites*, **31**(4) 213-220.
- 34 Ingham, J. P. (2009). Application of petrographic examination techniques to the assessment of  
35 fire-damaged concrete and masonry structures. *Materials characterization*, **60** 700-709.
- 36 ISO (834-1999) 834-1: 1999 fire resistance tests -elements of building construction- part I:  
37 General requirements. *Int Organ Stand.*
- 38 Kachanov, M. (1993). Elastic solids with many cracks and related problems. *Advances in*  
39 *applied mechanics*, **30** 259-445.
- 40 Khan, M. S., Prasad, J., Abbas, H. (2010). Shear strength of RC beams subjected to cyclic  
41 thermal loading. *Construction and building materials*, **24** 1869-1877.
- 42 Khan, M. S., Abbas, H. (2016). Performance of concrete subjected to elevated temperature.  
43 *European Journal of Environmental and Civil Engineering*, **20**(5) 532-543.
- 44 Kodur, V., Agrawal, A. (2017). Effect of temperature induced bond degradation on fire  
45 response of reinforced concrete beams. *Engineering Structures*, **142** 98-109.
- 46 Kong, X., Li, J. (2019). Non-contact fatigue crack detection in civil infrastructure through  
47 image overlapping and crack breathing sensing. *Automation in construction*, **99** 125-139.
- 48 Lam Dos-Santos, J., Rosa, L., Amaral, P. (2011). Temperature effects on mechanical behavior  
49 of engineered stones. *Construction and Building Materials*, **25**(1) 171-174.

- 1 Lataste, J., Sirieix, C., Breysse, D., Frappa, M. (2003). Electrical resistivity measurement  
2 applied to cracking assessment on reinforced concrete structures in civil engineering. *NDT & E*  
3 *International*, **36**(6) 383-394.
- 4 Li, B., Mao, J., Shen, W., Liu, H., Liu, X., Xu, G. (2019). Mesoscopic cracking model of  
5 cement based materials subjected to freeze-thaw cycles. *Construction and building materials*, **211**  
6 1050-1064.
- 7 Li, Z., Liu, Y., Huo, J., Rong, H., Chen, J., Elghazouli, A. Y. (2018). Experimental  
8 assessment of fire-exposed RC beam-column connections with varying reinforcement development  
9 lengths subjected to column removal. *Fire safety journal*, **99** 38-48.
- 10 Liu, S., Xu, J. (2015). An experimental study on the physico-mechanical properties of two  
11 post-high-temperature rocks. *Engineering Geology*, **185** 63-70.
- 12 Liu, J., Li, B., Tian, W., Wu, X. (2018). Investigating and predicting permeability variation in  
13 thermally cracked dry rocks. *International Journal of Rock Mechanics and Mining Sciences*, **103**  
14 77-88.
- 15 Mallet, C., Fortin, J., Guéguen, Y., Bouyer, F. (2013). Effective elastic properties of cracked  
16 solids: an experimental investigation. *International Journal of Fracture – Letters in Fracture and*  
17 *Micromechanics*, **182**(2).
- 18 Mallet, C., Fortin, J., Guéguen, Y., Bouyer, F. (2014). Evolution of the crack network in glass  
19 samples submitted to brittle creep conditions. *International Journal of Fracture*, **190**(1-2) 111-124.
- 20 Mindeguia, J.C., Pimienta, P., Noumowé, A., Kanema, M. (2010). Temperature, pore pressure  
21 and mass variation of concrete subjected to high temperature, experimental and numerical  
22 discussion on spalling risk. *Cement and Concrete Research*, **40**(3) 477-487.
- 23 Mollo, S., Heap, M. J., Dingwell, D. B., Hess, K. U., Iezzi, G., Masotta, M., Scarlato, P.,  
24 Vinciguerra, S. (2013). Decarbonation and thermal microcracking under magmatic P-T-CO<sub>2</sub>  
25 conditions: the role of skarn substrata in promoting volcanic instability. *Geophysical Journal*  
26 *International*, **195**(1) 369-380.
- 27 Motra, H. B., Zertani, S. (2018). Influence of loading and heating processes on elastic  
28 geomechanical properties of eclogites and granulites. *Journal of rock mechanics and geotechnical*  
29 *engineering*, **10**(1) 127-137.
- 30 Nasser, M., Schubnel, A., Benson, P., Young, R. (2009). Common evolution of mechanical  
31 and transport properties in thermally cracked westerly granite at elevated hydrostatic pressure. *Rock*  
32 *Physics and Natural Hazards*, **166**(5-7) 927-948.
- 33 NF-EN14066 (2013) Méthodes d'essai pour les pierres naturelles-Détermination de la  
34 résistance au vieillissement accéléré par choc thermique, B10-630.
- 35 Novák, J., Kohoutková, A. (2017). Fire response of hybrid fiber reinforced concrete to high  
36 temperature. *Procedia Engineering*, **172** 784-790.
- 37 Panza, E., Agosta, F., Rustichelli, A., Vinciguerra, S. C., Ougier-Simonin, A., Dobbs, M.,  
38 Prosser, G. (2019). Meso-to-microscale fracture porosity in tight limestones, results of an integrated  
39 field and laboratory study. *Marine and Petroleum Geology*, **103** 581-595.
- 40 Samouh, H., Rozière, E., Loukili, A. (2019). Experimental and numerical study of the relative  
41 humidity effect on drying shrinkage and cracking of self consolidating concrete. *Cement and*  
42 *concrete research*, **115** 519-529.
- 43 Sarker, P. K., Kelly, S., Yao, Z. (2014). Effect of fire exposure on cracking, spalling and  
44 residual strength of fly ash geopolymer concrete. *Materials and design*, **63** 584-592.
- 45 Schöpfer, M. P. J., Abe, S., Childs, C., Walsh, J. (2009). The impact of porosity and crack  
46 density on the elastic, strength and friction of cohesive granular materials: Insights from DEM  
47 modelling. *International Journal of Rock Mechanics and Mining Sciences*, **46** 250-261.
- 48 Shah, A. H., Sharma, U. K., (2017). Fire resistance and spalling performance of confined  
49 concrete columns. *Construction and building materials*, **156** 161-174.

1 Shapiro, S. M., O'Shea, D. C., Cummis, H. Z. (1967). Raman scattering study of the alpha-  
2 beta phase transition in quartz. *Physical review letters*, **19**(361).

3 Walsh, J. (1965a). The effect of cracks in rocks on poisson's ratio. *Journal of Geophysical*  
4 *Research*, **70**(20) 5249-5257.

5 Walsh, J. (1965b). The effect of cracks on the uniaxial elastic compression of rocks. *Journal*  
6 *of Geophysical Research*, **70**(2) 399-411.

7 Wang, G., Yang, D., Zhao, Y., Kang, Z., Kang, Z., Zhao, J., Huang, X. (2019). Experimental  
8 investigation on anisotropic permeability and its relationship with anisotropic thermal cracking of  
9 oil shale under temperature and triaxial stress. *Applied thermal engineering*, **146** 718-725.

10 Wang, XQ., Schubnel, A., Fortin, J., Guéguen, Y., Ge, H.K. (2013). Physical properties and  
11 brittle strength of thermally cracked granite under confinement. *Journal of Geophysical Research*,  
12 **118** 6099-6112.

13 Xing, Z., Beaucour, A.L., Hebert, R., Noumowe, A., Ledesert, B. (2011). Influence of the  
14 nature of aggregates on the behaviour of concrete subjected to elevated temperature. *Cement and*  
15 *concrete research*, **41**(4) 392-402.

16 Xiong, M. X., Liew, J. R. (2016). Mechanical behaviour of ultra-high strength concrete at  
17 elevated temperatures and fire resistance of ultra-high strength concrete filled steel tubes. *Materials*  
18 *& design*, **104** 414-427.

19 Yavuz, H., Altindag, R., Sarac, S., Ugur, I., Sengun, N. (2006). Estimating the index  
20 properties of deteriorated carbonate rocks due to freeze-thaw and thermal shock weathering.  
21 *International Journal of Rock Mechanics and Mining Sciences*, **43**(5) 767-775.

22 Yermak, N., Pliya, P., Beaucour, A. L., Simon, A., Noumowé, A. (2017). Influence of steel  
23 and/or polypropylene fibres on the behaviour of concrete at high temperature: Spalling, transfer and  
24 mechanical properties. *Construction and Building Materials*, **132** 240-250.

25 Zhang, Y., Sun, Q., Geng, J. (2017). Microstructural characterization of limestone exposed to  
26 heat with XRD, SEM and TG-DSC. *Materials characterization*, **134** 285-295.

27 Zhang, F., Zhao, J., Hu, D., Skoczylas, F., Shao, J. (2018). Laboratory investigation on  
28 physical and mechanical properties of granite after heating and water-cooling treatment. *Rock*  
29 *Mechanics and Rock Engineering*, **51**(3) 677-694.

30  
31  
32  
33  
34  
35  
36  
37  
38  
39